The Astronomical Journal, 129:1–8, 2005 January

X-RAY PROPERTIES OF LYMAN BREAK GALAXIES IN THE GREAT OBSERVATORIES ORIGINS DEEP SURVEY

B. D. Lehmer,[1] W. N. Brandt,[1] D. M. Alexander,[2] F. E. Bauer,[2] C. J. Conselice,[3] M. E. Dickinson,[4] M. Giavalisco,[5] N. A. Grogin,[6] A. M. Koekemoer,[5] K.-S. Lee,[5,6] L. A. Moustakas,[5] and D. P. Schneider[1]

Received 2004 August 13; accepted 2004 September 21

ABSTRACT

We constrain the X-ray emission properties of Lyman break galaxies (LBGs) at $z \approx 3$–6 using the ≈2 Ms Chandra Deep Field North and ≈1 Ms Chandra Deep Field South. Large samples of LBGs were discovered using the *Hubble Space Telescope* as part of the Great Observatories Origins Deep Survey (GOODS). Deep optical and X-ray imaging over the GOODS fields have allowed us to place the most significant constraints on the X-ray properties of LBGs to date. Mean X-ray properties of 449, 1734, 629, and 247 LBGs with $z \sim 3$, 4, 5, and 6, respectively, were determined using stacking techniques. When stacked, we detect X-ray emission from LBGs at $z \sim 3$ ($\sim 7\ \sigma$) and from an optically bright subset (brightest 25%) of LBGs at $z \sim 4$ ($\sim 3\ \sigma$); the latter is the highest redshift detection yet for "normal" galaxies in the X-ray band. The effective exposure times for these stacked observations are ≈0.7 and 0.5 Gs, respectively. The derived average rest-frame 2.0–8.0 keV luminosities are 1.5×10^{41} and 1.4×10^{41} ergs s^{-1}, respectively. X-ray emission from these LBGs is likely due to high-mass X-ray binaries and Type II supernovae; the corresponding star formation rates are ≈10–30 $M_{\odot}$ yr^{-1}. The X-ray–to–*B*-band mean luminosity ratio (L_X/L_B) at $z \sim 3$ is somewhat elevated with respect to that measured for starburst galaxies in the local universe (significance $\sim 3\ \sigma$). When stacking full samples of LBGs at $z \sim 4$, 5, and 6, we do not obtain significant detections ($<3\ \sigma$) and derive rest-frame 2.0–8.0 keV luminosity upper limits ($3\ \sigma$) of 0.9, 2.8, and 7.1×10^{41} ergs s^{-1}, respectively. These upper limits constrain any widespread active galactic nucleus (AGN) activity in these objects to be modest at best. Furthermore, we find that ∼0.5% of our LBGs from $z \approx 3$ to $z \approx 6$ are detected individually in the X-ray band. These LBGs have spectral shapes and luminosities characteristic of moderate-power AGNs (e.g., Seyfert galaxies and quasars).

Key words: cosmology: observations — surveys — X-rays: galaxies — X-rays: general

1. INTRODUCTION

Determination of the basic X-ray properties of "normal" galaxies (i.e., not hosting a luminous active galactic nucleus [AGN]) out to high redshift has been motivated in part by Ghosh & White (2001, hereafter GW01), who developed a model of the evolution of X-ray luminosity with redshift. GW01 predict that, globally, X-ray emission from normal galaxies should peak at $z \approx 1.5$–3 as the result of a maximum in the global star formation rate (SFR) at $z \approx 2.5$–3.5 (e.g., Blain et al. 1999). Heightened X-ray emission at these redshifts is expected because of an increase in the global population of low-mass X-ray binaries (LMXBs). LMXBs evolve on timescales of ∼1 Gyr, and therefore their X-ray signatures should lag behind more immediate tracers of star formation.

Stacking analyses and deep X-ray surveys with the *Chandra X-Ray Observatory* have enabled testing of these predictions out to cosmologically interesting distances. Stacking techniques generally involve the addition of X-ray counts at known positions of galaxies to yield average X-ray detections where individual sources lie below the detection threshold. For example, Hornschemeier et al. (2002) used stacking with a ≈1 Ms exposure of the Chandra Deep Field North (CDF-N) to investigate the evolution of the X-ray luminosities of $z = 0.4$–1.5 spiral galaxies. This analysis shows suggestive evidence for evolution in X-ray luminosity with redshift at a level somewhat lower than that predicted by GW01. Hornschemeier et al. also found that the X-ray–to–*B*-band luminosity ratio, L_X/L_B, is elevated for $z \approx 1$ spirals with rest-frame $L_B \approx L_B^*$ as compared with galaxies in the local universe. More recent stacking analyses of large samples of galaxies in the ≈2 Ms CDF-N and ≈1 Ms Chandra Deep Field South (CDF-S) show that the X-ray properties of normal galaxies of all morphological types evolve similarly from $z = 0.4$ to 1.5 (Wu et al. 2005).

At higher redshifts ($z \approx 2$–6), stacking analyses have been performed using individually undetected normal galaxies (e.g., Brandt et al. 2001, hereafter B01; Nandra et al. 2002, hereafter N02; Malhotra et al. 2003; Bremer et al. 2004; Moustakas & Immler 2004; Reddy & Steidel 2004; Wang et al. 2004). At $z \sim 3$ these galaxies often have mean X-ray luminosities and L_X/L_B comparable to bright starburst galaxies in the local universe. The heightened X-ray emission from these galaxies is probably due to newly formed high-mass X-ray binaries (HMXBs) and young supernova remnants. HMXBs have much shorter formation timescales than LMXBs and are therefore more immediate tracers of cosmic star formation history.

Recently, large samples of galaxies have been identified at $z \sim 3$, 4, 5, and 6 as part of the Great Observatories Origins Deep Survey (GOODS). These galaxies were isolated by means of the Lyman break technique (see, e.g., Madau et al. 1996;

[1] Department of Astronomy and Astrophysics, 525 Davey Lab, Pennsylvania State University, University Park, PA 16802.
[2] Institute of Astronomy, Madingley Road, Cambridge CB3 0HA, UK.
[3] Palomar Observatory, California Institute of Technology, Pasadena, CA 91125.
[4] National Optical Astronomy Observatory, 950 North Cherry Avenue, Tucson, AZ 85719.
[5] Space Telescope Science Institute, 3700 San Martin Drive, Baltimore, MD 21218.
[6] Department of Physics and Astronomy, Johns Hopkins University, 3400 North Charles Street, Baltimore, MD 21218-2686.

Steidel et al. 1999), which estimates the redshift of a galaxy based on its "dropout" bandpass (see § 2.1). Lyman break galaxies (LBGs) generally show rest-frame UV/optical characteristics similar to those of local starburst galaxies—weak or absent Lyα emission, P Cygni profiles, and stellar absorption features from Si IV, C IV, and He II (see, e.g., Steidel et al. 1996; Shapley et al. 2003). The GOODS covers $\approx$316 arcmin^2 of sky in two fields, GOODS North (GOODS-N) and GOODS South (GOODS-S) (Giavalisco et al. 2004b). Both fields are subregions of the Chandra Deep Fields for which *Chandra* has acquired an $\approx$2 Ms observation of the CDF-N (Alexander et al. 2003, hereafter A03) and an $\approx$1 Ms observation of the CDF-S (Giacconi et al. 2002; A03).

In this paper, we use stacking techniques to constrain the X-ray properties of LBGs in the GOODS fields. We improve on results from B01 and N02 by increasing the number of galaxies at $z \sim 3$ from 24 (B01) and 148 (N02) to 449, and we add to this samples of 1734, 629, and 247 galaxies at $z \sim 4$, 5, and 6, respectively.

The Galactic column densities are 1.3×10^{20} cm^{-2} (Lockman 2004) and 8.0×10^{19} cm^{-2} (Stark et al. 1992) for the CDF-N and CDF-S, respectively. $H_0 = 70$ km s^{-1} Mpc^{-1}, $\Omega_m = 0.3$, and $\Omega_\Lambda = 0.7$ are adopted throughout this paper (Spergel et al. 2003). Coordinates are J2000.0.

2. ANALYSIS

2.1. *Samples*

The Lyman break technique has been utilized in the GOODS regions, where deep mosaic images have been taken using the *Hubble Space Telescope* Advanced Camera for Surveys (ACS) with bandpasses B_{435}, V_{606}, i_{775}, and z_{850} (Giavalisco et al. 2004a, hereafter G04a). Additional ground-based photometry has been obtained over the GOODS fields in the U band at KPNO (Capak et al. 2004, GOODS-N) and CTIO (GOODS-S). LBGs that drop out of the bandpasses U, B_{435}, V_{606}, and i_{775} correspond to objects with z of 3.01 ± 0.24, 3.78 ± 0.34, 4.92 ± 0.33, and 5.74 ± 0.36, respectively.[7] Identification of these LBGs is based on the following color equations as defined by G04a.

U dropouts:

$$U - B_{450} \geq 0.75 + 0.5(B_{450} - z_{850})$$
$$U - B_{450} \geq 0.9 \qquad B_{450} - z_{850} \leq 4.0. \tag{1}$$

B_{435} dropouts:

$$B_{450} - V_{606} \geq 1.2 + 1.4(V_{606} - z_{850})$$
$$B_{450} - V_{606} \geq 1.2 \qquad V_{606} - z_{850} \leq 1.2. \tag{2}$$

V_{606} dropouts:

$$V_{606} - i_{775} > 1.5 + 0.9(i_{775} - z_{850})$$
$$V_{606} - i_{775} > 2.0 \quad V_{606} - i_{775} \geq 1.2 \quad i_{775} - z_{850} \leq 1.3. \tag{3}$$

i_{775} dropouts:

$$i_{775} - z_{850} \geq 1.3. \tag{4}$$

[7] These error bars are the 1 σ statistical errors for redshift measurements.

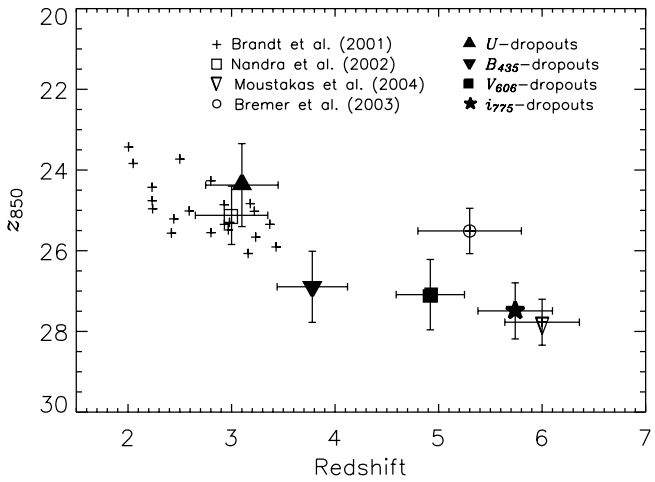

FIG. 1.—Plot of the z_{850} magnitude vs. redshift for X-ray stacking analyses of LBGs. Filled (our LBGs) and open symbols (other investigations) represent the estimated mean z_{850} and redshift, with error bars showing the 1 σ spread for each quantity. The Brandt et al. (2001) measurements (*plus signs*) represent the positions of individual LBGs with spectroscopic redshifts.

Here the symbols $\wedge$ and $\vee$ correspond to the logical operators AND and OR, respectively. Dropout lists created by G04a were inspected and filtered to minimize the number of interlopers and contaminants in the samples. The interloper fraction is predicted to be $\approx$10% for U and B_{435} dropouts. This fraction increases to become significant for V_{606} and i_{775} dropouts ($\approx$20% and 40%, respectively; see Dickinson et al. 2004; G04).

The LBGs used in our stacking analyses have average redshifts and z_{850} magnitudes as shown in Figure 1; for comparison, the z_{850} magnitudes of several other stacking analyses in this redshift range are also plotted. Galaxies in this survey probe relatively faint optical fluxes over a wider range of redshifts ($z \approx 3$–6) than those used for previous X-ray stacking analyses. The corresponding look-back times for U, B_{435}, V_{606}, and i_{775} dropouts are 11.5, 12.1, 12.5, and 12.7 Gyr, respectively (see Hogg 2000).

The stacking procedure used in our analyses was similar to that of B01 and N02; the intent was to obtain average X-ray properties (e.g., luminosities and spectral shapes). At each LBG position, photon counts and effective exposure times (from exposure maps, which include the effects of vignetting) were extracted from circular apertures and summed to give a total number of counts and a total effective exposure time. We excluded LBGs located within 10″ of individually detected X-ray sources in A03; this avoids contamination by unrelated sources. This exclusion process led to the rejection of 99, 267, 127, and 31 U, B_{435}, V_{606}, and i_{775} dropouts, respectively ($\approx$18%, 13%, 17%, and 11% of the respective LBG populations). A small number of LBGs (18) were found to be within the positional errors of *Chandra* sources; their characteristics are given in § 3.1 and listed in Table 1.

The background was estimated through Monte Carlo analysis using a background map (see § 4.2 of A03). Each LBG position was shifted randomly within 25″ of the original position, and background counts were obtained for each new position and summed just as they were for the LBGs themselves. This procedure was repeated 10,000 times to obtain an accurate estimate of the local background and its dispersion. To verify our results were not biased by gradients in the local background, we also tried shifting in regions with radii of 10″, 15″, 20″, 30″, and 35″ and found no material differences in our results.

TABLE 1
INDIVIDUALLY DETECTED LBGs

Chandra Name (J2000) (1)	Dropout Bandpass (2)	Position Error (arcsec) (3)	Offset (arcsec) (4)	z (5)	Counts SB (6)	$f_{0.5-2\ \mathrm{keV}}$ (10^{-16} ergs cm^{-2} s^{-1}) (7)	$f_{2-8\ \mathrm{keV}}$ (10^{-16} ergs cm^{-2} s^{-1}) (8)	Γ (9)	$L_{2-8\ \mathrm{keV}}$ (10^{43}ergs s^{-1}) (10)	z_{850} (11)
J033201.6−274327.....	U	0.4	0.15	2.726[s]	450.7	27.7	56.2	1.5	14.9	23.8
J033209.4−274807.....	U	0.3	0.10	2.81[s]	195.6	11.0	59.7	0.8	6.4	22.4
J033218.2−275241.....	U	0.6	0.10	2.801[s]	55.9	3.6	6.3	1.6	2.1	24.1
J033222.2−274937.....	B_{435}	0.6	0.19	...	10.1	0.6	<3.8	1.4	0.7	27.5
J033229.8−275106.....	B_{435}	0.6	0.14	3.700[s]	53.5	3.1	31.8	0.4	3.4	24.8
J033238.8−275122.....	B_{435}	0.6	0.25	...	16.2	1.1	8.9	0.6	1.3	26.3
J033239.1−274439.....	B_{435}	0.6	0.24	...	76.2	4.6	21.0	0.9	5.4	28.0
J033239.7−274851.....	B_{435}	0.3	0.14	3.064[s]	134.6	7.5	7.1	0.4	5.3	24.8
J033242.8−274702.....	B_{435}	0.6	0.13	3.193[s]	112.0	6.3	16.4	1.3	5.0	25.2
J033243.2−274914.....	U	0.3	0.02	1.92[s]	621.4	36.6	61.1	1.7	8.4	24.2
J033244.3−275251.....	U	0.7	0.29	3.471[s]	85.4	5.4	6.8	1.9	5.2	24.2
J033250.2−275252.....	B_{435}	0.4	0.33	3.6[p]	404.2	24.0	75.3	1.2	25.1	26.1
J123621.0+621412.....	U	0.6	0.16	1.74[p]	131.9	3.7	6.0	1.7	0.7	25.4
J123642.2+620612.....	B_{435}	0.4	0.39	0.70[p]	126.4	3.9	12.6	1.2	0.1	26.4
J123647.9+621020.....	V_{606}	0.6	0.26	...	28.1	0.8	19.4	>0.3	1.7	27.3
J123648.0+620941.....	V_{606}	0.6	0.23	5.186[s]	96.7	2.7	4.9	1.6	6.7	23.8
J123701.6+621146.....	i_{775}	0.6	0.43	1.52[p]	13.9	0.4	<1.2	1.4	0.1	27.8
J123714.3+621208.....	U	0.6	0.14	3.146[s]	74.0	2.2	5.2	1.4	1.7	25.5

NOTES.—Col. (1): *Chandra* source name. Col. (2): Observed ACS dropout bandpass. Col. (3): Positional error as reported in A03. Col. (4): Angular offset between positions determined by *Chandra* and ACS. Col. (5): Spectroscopic ("s") or photometric ("p") redshift. Col. (6): Soft-band X-ray counts. Col. (7): Soft-band flux. Col. (8): Hard-band flux. Col. (9): Effective photon index. Here a value of 1.4 was assumed when photon statistics were too low to determine accurate values. Col. (10): Hard-band X-ray luminosity. Col. (11): z_{850}-band magnitude.

Our stacking procedure maximized the signal-to-noise ratio (S/N)[8] by varying the aperture cell size for extracting X-ray counts and the off-axis angle (angle between a particular source and the average CDF-N or CDF-S aim points) within which sources were included in stacking. This procedure was performed using U dropouts because of their strong X-ray signal. We avoided stacking sources that were outside a certain off-axis angle due to the increased size of the point-spread function (PSF) and confusion with background in this region. In the maximization process we chose a specific aperture cell size and stacked sources within various off-axis angles (hereafter inclusion radii) until S/N was maximized. Sources within the resulting inclusion radius were then stacked using variable aperture cell sizes. The S/N was maximized for a specific aperture cell size, and the process was repeated iteratively until convergence. Figures 2*a* and 2*b* show the result of this process. We found that S/N peaks for an inclusion radius $\approx 9\farcm0$ and an aperture size of $\approx 1\farcs5$ (as expected for small off-axis angles); these values are used throughout our analyses.

Mean count rates Φ were calculated by subtracting our best estimate of the local background counts B from the background plus source counts S and dividing by the total effective exposure time T [i.e., $\Phi = (S - B)/T$]. To convert count rate to flux, we used the Galactic column densities discussed in § 1 and adopted a power-law photon index of $\Gamma = 2.0$, appropriate for starburst galaxies (e.g., Kim et al. 1992; Ptak et al. 1999). Sources were stacked in both the GOODS-N and GOODS-S fields, so we used a statistically weighted Galactic column density. X-ray luminosities were calculated following Schmidt & Green (1986):

$$L_{\mathrm{X}} = 4\pi d_L^2 f_{\mathrm{X}} (1+z)^{\Gamma-2}\ \mathrm{ergs\ s^{-1}}, \tag{5}$$

where d_L is the luminosity distance in centimeters and f_{X} is the X-ray flux (ergs cm^{-2} s^{-1}).

2.2. *Subsets*

The large number of LBGs in our sample enabled investigation of the contribution of specific subsets to the signal. We chose to divide the original dropout lists based on galaxy morphology (U dropouts only) and rest-frame B-band luminosity. We used the *CAS* morphology system (Conselice 2003) to divide the U-dropout list according to the observed-frame z_{850}-band (rest-frame wavelengths 1000–2500 Å from $z \approx 3$ to 6) concentration and asymmetry parameters. Concentration (C) is proportional to the logarithm of the ratio of the radii containing 80% and 20% of the source flux:

$$C = 5 \log \left(r_{80\%} / r_{20\%} \right). \tag{6}$$

Galaxies with high C-values (e.g., bulge-dominated systems) are generally brightest in their central regions (Conselice et al. 2002). Asymmetry (A) is defined for a galaxy by taking the absolute value of the difference in fluxes of the galaxy's image and its 180° rotated analog and dividing by the original image flux (see Conselice et al. 2000 and Conselice 2003 for details). Generally, disk-dominated systems and galaxy mergers are observed to have high A-values. Values of $A = 0.1$ and $C = 2.7$ were chosen to divide the U-dropout list roughly in half, resulting in lists of LBGs with $A < 0.1$, $A > 0.1$, $C < 2.7$, and $C > 2.7$.

We also divided our original dropout lists into subsets based on rest-frame B-band luminosity. Rest-frame B-band luminosities

[8] Here $\mathrm{S/N} \equiv (S - B)/B^{0.5}$, where S is the source plus background counts and B is the average background counts obtained from the Monte Carlo procedure. This approximation is accurate for $|S - B| \ll B$ and $B \geq 20$, which applies to all cases in our analyses.

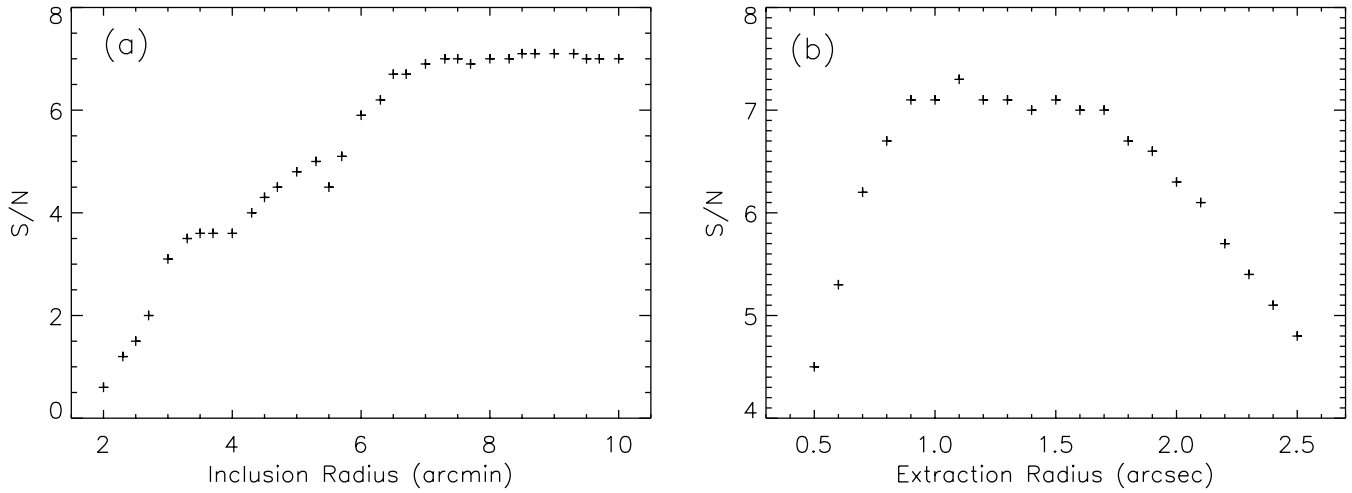

FIG. 2.—(*a*) Achieved signal-to-noise ratio (S/N) as a function of inclusion radius for stacking *U* dropouts. Note that the number of stacked sources rises with increasing inclusion radius and is maximized at $\approx 9\farcm0$. (*b*) Signal-to-noise ratio (S/N) as a function of extraction radius. Here the signal is strongest for an aperture radius of $\approx 1\farcs5$. This process of optimizing the S/N was achieved iteratively and appears here in convergence.

were calculated using a spectral energy distribution (SED) and applying *K*-corrections to the fluxes (e.g., Schneider et al. 1983; Hogg et al. 2002). *K*-corrected ACS magnitudes were used in these computations; thus, the derived rest-frame *B*-band luminosities are strongly dependent on the SED choice. An SED for LBGs was used in calculating *K*-corrections. This SED was derived from the Bruzual & Charlot (2003) solar metallicity models, with a Salpeter initial mass function, and aged by 144 Myr at constant SFR. Optically bright and faint sublists were generated by dividing each dropout list (i.e., U, B_{435}, V_{606}, and i_{775} dropouts) at its mean rest-frame *B*-band luminosity. The corresponding mean rest-frame *B*-band luminosities used in these divisions were $L_B \approx 5.3, 5.5, 4.1$, and 5.5×10^{43} ergs s^{-1} ($M_B \approx -20.6, -20.5, -20.1, -20.6$) for U, B_{435}, V_{606}, and i_{775} dropouts, respectively. Because rest-frame *B*-band luminosity distributions are asymmetric with skew tails toward high luminosity, splitting at the mean leads to two lists of unequal size.

3. RESULTS

3.1. *Detected Sources*

Over the GOODS fields, seven U dropouts, eight B_{435} dropouts, two V_{606} dropouts, and one i_{775} dropout were found to be coincident with *Chandra* sources within the positional errors (see Table 1).[9] Positional errors, photon counts, effective photon indices, and fluxes for these sources were determined in A03. The 2.0–8.0 keV X-ray luminosities were computed using equation (5).[10] We investigated the probability of obtaining a false match by shifting all of our LBG positions and checking to see whether the new positions were coincident with *Chandra* sources. LBG positions were shifted by $10''$ in 16 different directions, and an average of approximately two detections were obtained for each direction.

Of the 18 detected sources, we find that 14 have corresponding spectroscopic (Barger et al. 2003b; Cristiani et al. 2004; Mobasher et al. 2004; Szokoly et al. 2004; Zheng et al. 2004) and/or photometric (Barger et al. 2003b) redshifts. Of these 14 sources, two (J123642.2+620612 and J123701.6+621146) have redshifts inconsistent with those determined by the Lyman break technique. We note that the redshifts for these sources have been derived photometrically, implying there are still uncertainties in their values. Furthermore, these sources may also be interlopers (see § 2.1 for probabilities) or falsely matched.

The detected sources are mostly active galactic nuclei (AGNs) with moderate luminosities (i.e., $L_X \approx 10^{43}$–$10^{44.5}$ ergs s^{-1}), characteristic of luminous Seyfert-type galaxies to quasars. Several of these sources have been characterized in previous investigations. J123648.0+620941 is the highest redshift quasar known ($z = 5.186$) in the CDF-N and CDF-S fields (e.g., Barger et al. 2003a; Vignali et al. 2002). J033201.6−274327, J033218.2− 275241, J033243.2−274914, J033244.3−275251 (Szokoly et al. 2004), and J033209.4−274807 (Schreier et al. 2001) have been spectroscopically classified as broad-line AGNs. J123701.6+621146 and J123647.9+620941 are both very red objects (VROs: $I-K \geq 4$; Alexander et al. 2002b). J033229.8−275105 has been identified as a putative type 2 QSO (Norman et al. 2002). Finally, three additional sources (J033239.7−274851, J033242.8−274702, and J033250.2−275252) have been cataloged as high-redshift QSO candidates (Cristiani et al. 2004).

Following Alexander et al. (2002a), we assume that detected sources with 2.0–8.0 keV $L_X > 1.5 \times 10^{42}$ ergs s^{-1} or $\Gamma < 1.0$ are AGNs. Only one source (J123642.2+620612) falls outside these criteria, leaving 17 clear AGNs. The derived AGN fractions for our U, B_{435}, V_{606}, and i_{775} dropouts are $\approx 1.2\%$, 0.4%, 0.3%, and 0.4%, respectively; these fractions are lower than others found in previous investigations. For comparison, the AGN fraction derived from N02 is $\approx 2.7\%$. In comparison to our B_{435}, V_{606}, and i_{775} dropouts, our U dropouts and the LBGs used by N02 are relatively luminous in the optical. The corresponding AGN fractions therefore suggest that X-ray–luminous AGNs are generally optically luminous as well.

3.2. *Stacked Sources*

The results of our stacking analyses of individually undetected sources are found in Table 2. Hereafter, unless stated

[9] Note that the Lyman break technique is a statistical process for isolating galaxies at a given redshift. Because of the statistical nature of this process, we do not expect to recover all objects within the ACS flux limits that may reside at the redshifts under investigation here.

[10] For reference, the on-axis sensitivity limit for the 2 Ms CDF-N is $\approx 2.5 \times 10^{-17}$ ergs cm^{-2} s^{-1} in the soft band, corresponding to rest-frame 2.0–8.0 keV luminosities of 2.0, 4.0, 6.8, and 10.4×10^{42} ergs s^{-1} at $z = 3$, 4, 5, and 6, respectively ($\Gamma = 2$).

TABLE 2

STACKING RESULTS FOR FILTERED DROPOUT LISTS

Data Type (1)	N (2)	S (3)	B (4)	σ (5)	S/N (6)	E (Ms) (7)	$N_{\rm trials} > S$ (8)	Φ (10^{-7} counts s^{-1}) (9)	$f_{\rm X}$ (10^{-18} ergs cm^{-2} s^{-1}) (10)	$L_{\rm X}$ (10^{41} ergs s^{-1}) (11)	L_B (10^{43} ergs s^{-1}) (12)	log ($L_{\rm X}/L_B$) (13)
						U Dropouts ($z \sim 3$)						
General.....	449	1351.0	1115.3	33.4	7.1	663.9	0	3.6 ± 0.7	1.9 ± 0.4	1.5 ± 0.3	5.3	-2.6 ± 0.2
Bright	201	589.2	462.4	21.5	5.9	274.8	0	4.6 ± 1.2	2.4 ± 0.6	1.9 ± 0.5	10.3	-2.7 ± 0.3
Dim	248	759.7	651.9	25.5	4.2	389.2	0	2.8 ± 1.0	1.5 ± 0.5	1.2 ± 0.4	3.1	-2.4 ± 0.3
$C > 2.7$	223	672.0	559.4	23.7	4.8	332.7	0	3.4 ± 1.1	1.8 ± 0.6	1.4 ± 0.4	4.5	-2.5 ± 0.3
$C \leq 2.7$.....	226	676.8	555.2	23.6	5.2	331.2	0	3.7 ± 1.1	1.9 ± 0.6	1.5 ± 0.4	6.1	-2.6 ± 0.3
$A > 0.1$.....	213	671.3	524.1	22.9	6.4	312.7	0	4.7 ± 1.1	2.5 ± 0.6	2.0 ± 0.5	6.7	-2.5 ± 0.2
$A \leq 0.1$.....	236	677.5	591.0	24.3	3.6	351.2	0	2.5 ± 1.0	1.3 ± 0.5	1.0 ± 0.4	4.3	-2.6 ± 0.4
						B_{435} Dropouts ($z \sim 4$)						
General.....	1734	3749.5	3625.7	60.2	2.1	2102.2	197	$\lesssim 1.2$	$\lesssim 0.6$	$\lesssim 0.9$	2.9	$\lesssim -2.4$
Bright	395	925.5	832.9	28.9	3.2	485.5	6	1.9 ± 0.9	1.0 ± 0.5	1.4 ± 0.6	9.2	-2.8 ± 0.5
Dim	1339	2823.8	2793.6	52.9	0.6	1616.8	2783	$\lesssim 1.4$	$\lesssim 0.7$	$\lesssim 1.0$	2.1	$\lesssim -2.7$
						V_{606} Dropouts ($z \sim 5$)						
General.....	629	1382.0	1373.7	37.1	0.2	804.9	4067	$\lesssim 2.0$	$\lesssim 1.0$	$\lesssim 2.8$	2.6	$\lesssim -2.8$
						i_{775} Dropouts ($z \sim 6$)						
General.....	247	533.3	505.5	22.5	1.2	296.0	1065	$\lesssim 3.3$	$\lesssim 1.7$	$\lesssim 7.1$	3.7	$\lesssim -1.8$

NOTES.—The data apply to stacking analyses in the soft band. Col. (1): Description of the LBG sample stacked. "Bright" and "Dim" subsets were created by splitting the "General" lists at rest-frame B-band luminosities $\approx 5.3 \times 10^{43}$ and 5.5×10^{43} ergs s^{-1} ($M_B \approx -20.6$ and -20.5) for U and B_{435} dropouts, respectively. Col. (2): Number of sources being stacked. Col. (3): X-ray source counts obtained from stacking. Col. (4): Mean background counts obtained from Monte Carlo simulations. Col. (5): Poisson error of the background $B^{0.5}$. Col. (6): Signal-to-noise ratio $(S - B)/B^{0.5}$. Col. (7): Total, stacked effective exposure time. Col. (8): Number of Monte Carlo trials (out of 10,000) that produced a background estimate above S. Col. (9): X-ray count rate. Col. (10): X-ray (0.5–2.0 keV) flux. Col. (11): 2–8 keV rest-frame luminosity. Col. (12): Rest-frame B-band luminosity. Col. (12): Logarithm of X-ray to B-band luminosity ratio.

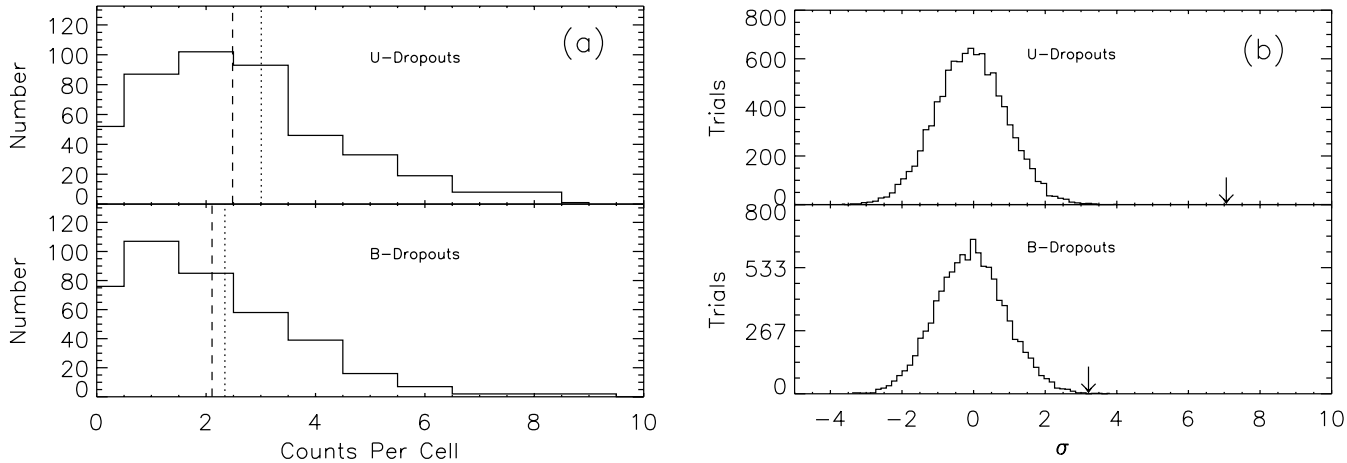

FIG. 3.—(*a*) Histogram of the count distribution for *U* dropouts (*top*) and B_{435} dropouts (*bottom*). The vertical dotted lines show the mean source plus background counts per aperture cell, and the vertical dashed lines show the mean background counts per aperture cell. (*b*) Results from Monte Carlo estimates of the background level for *U* dropouts (*top*) and B_{435} dropouts (*bottom*). The detection level is represented by downward-pointing arrows.

otherwise we discuss the results in reference to the soft-band stacking analyses, where we obtain significant detections; we do not obtain significant detections in the hard or full bands (this result is understandable because of the significantly lower background in the soft band). The stacking procedure was repeated for the GOODS-N and GOODS-S fields individually; results from the two fields were statistically consistent. Generally, we detect the stacked emission from *U* dropouts ($\sim$7 σ) and all subsets generated from them. We do not obtain significant detections (S/N > 3 σ) for general samples of B_{435}, V_{606}, and i_{775} dropouts, but we do obtain a significant detection for the bright subset of B_{435} dropouts ($\sim$3 σ). Figure 3*a* shows the distributions of counts obtained for the individual galaxies being stacked for both *U* dropouts and the bright subset of B_{435} dropouts. We obtained an average of 3.1 and 2.3 counts per cell for *U* and bright B_{435} dropouts, respectively. The summed numbers of source plus background counts were 1351 counts for *U* dropouts and 926 for bright B_{435} dropouts. In the 10,000 Monte Carlo trials in which we shifted the aperture cells to random positions and summed background counts, we found that no trials produced $\gtrsim$1351 counts for *U* dropouts and only six trials produced $\gtrsim$926 counts for B_{435} dropouts. Gaussian statistics predict that $\approx$0 and 5 Monte Carlo trials should exceed the total source+background counts for our analysis of *U* and bright B_{435} dropouts, respectively. Figure 3*b* shows the Monte Carlo distributions obtained when stacking random positions over 10,000 trials. In both cases the detection confidence levels are greater than 99.9%. Stacked and smoothed images are displayed in Figure 4. The images have effective exposure times of $\approx$0.7 and 0.5 Gs (22 and 16 yr) for *U* and bright B_{435} dropouts, respectively.

Stacked V_{606} and i_{775} dropouts and subsets thereof produced no significant detections (i.e., S/N < 3 σ). We also attempted to merge the bright subsets of V_{606} and i_{775} dropouts and failed to

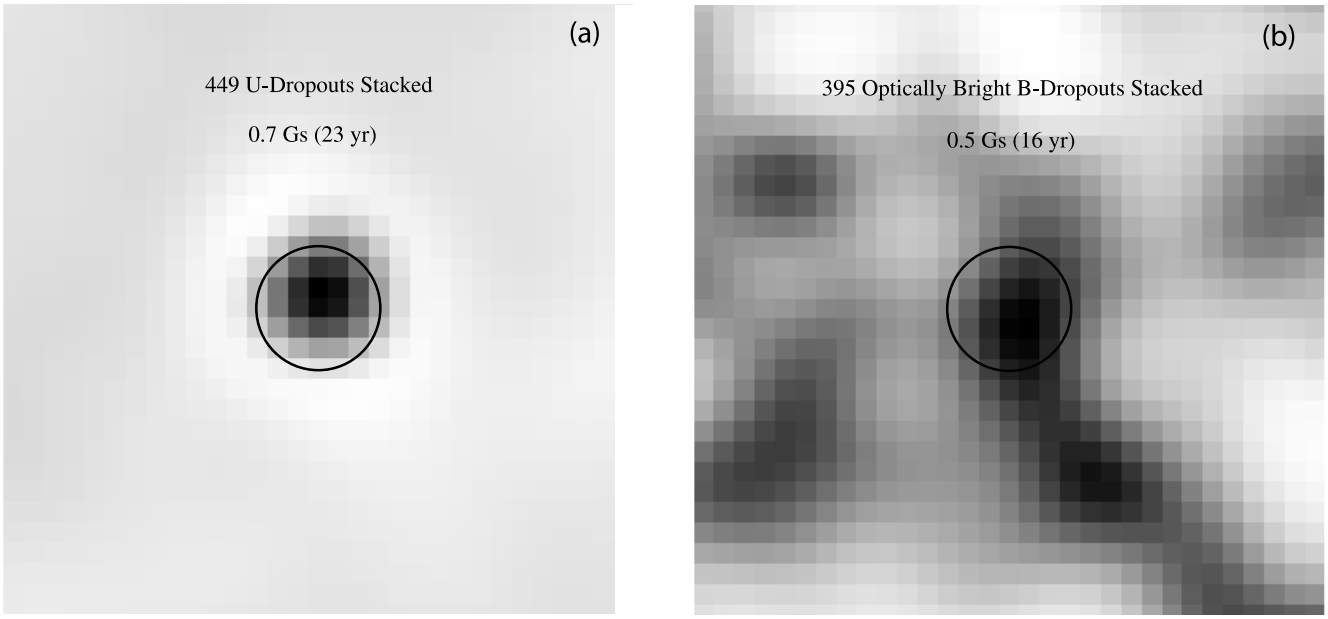

FIG. 4.—Stacked soft-band images of (*a*) 449 *U* dropouts ($\approx$0.7 Gs exposure) and (*b*) 395 optically bright B_{435} dropouts ($\approx$0.5 Gs exposure). Stacked emission from these LBGs is significantly detected in the soft band, with significances of $\sim$7 σ (*U* dropouts) and $\sim$3 σ (bright B_{435} dropouts). The images are $15'' \times 15''$ ($0\farcs5$ pixel^{-1}) and were adaptively smoothed at 2.5 σ using the CIAO tool CSMOOTH. The faint "nebulosity" observed in the optically bright B_{435} dropouts is attributed to smoothing over noise. The black circles are centered on our $1\farcs5$ radius aperture cell that was used in the stacking analyses.

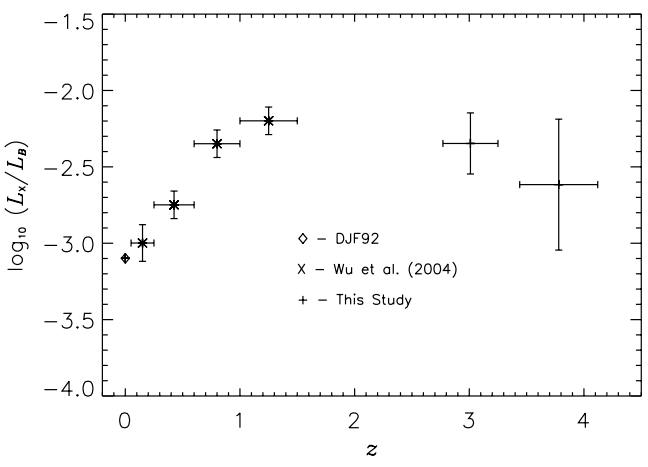

FIG. 5*a*

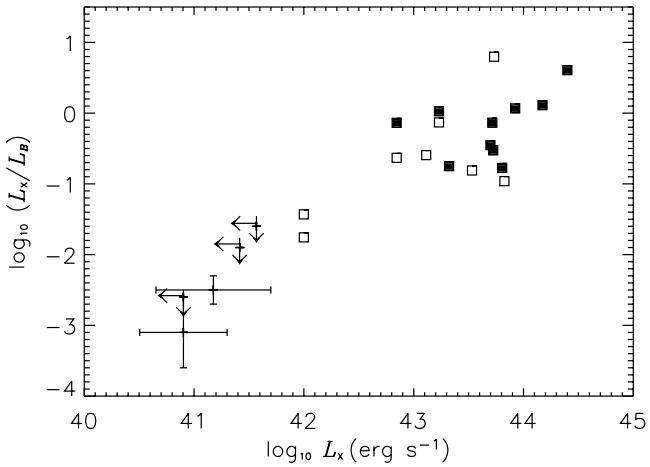

FIG. 5*b*

FIG. 5.—(*a*) X-ray (0.5–4.5 keV) to *B*-band luminosity ratio vs. redshift. Note that the suggested maximum of L_X/L_B at $z \sim 1.5$–3 is consistent with predictions from the cosmic star formation history. Data used in this figure come from the following sources: $z \sim 0$ (DJF92), $z \sim 0.05$–1.5 (Wu et al. 2005), $z \sim 3$ and 4, our *U* and B_{435} dropouts, respectively. (*b*) X-ray to *B*-band luminosity ratio vs. X-ray luminosities of individually undetected stacked LBGs (*plus signs*) and individually detected LBGs (*squares*); filled squares represent broad-line AGNs. The individually detected sources are AGNs (with one possible exception) and have much larger L_X/L_B ratios than our stacked LBGs. X-ray luminosities were calculated assuming a power law with photon index $\Gamma = 2$, and *B*-band luminosities were computed using *K*-corrections with an LBG SED (see § 2.2).

obtain detections. X-ray emission constraints for these LBGs are tabulated in Table 2.

4. DISCUSSION

Using the ≈2 Ms CDF-N plus ≈1 Ms CDF-S, we have placed constraints on the X-ray properties of LBGs identified in the 316 arcmin^2 GOODS-N and GOODS-S fields. We have used X-ray stacking techniques on samples of 449, 1734, 629, and 247 individually undetected LBGs at $z \sim 3$, 4, 5, and 6, respectively (*U*, B_{435}, V_{606}, and i_{775} dropouts, respectively) to obtain their average X-ray properties. X-ray emission from LBGs is expected to be largely due to activity associated with star-forming processes (e.g., HMXBs and young supernova remnants), with a low-level contribution from low-luminosity AGNs (e.g., Ho et al. 2001). With the intent of investigating normal/starburst galaxies, we have rejected LBGs coincident with known *Chandra* sources from our stacking analyses. Considering *Chandra*'s superb sensitivity for detecting luminous AGNs, we are confident that this rejection process has effectively removed strong accretion-dominated X-ray sources that would heavily contaminate our stacked signal. We have identified 18 LBGs coincident with *Chandra* sources (see § 3.1). With the possible exception of one source, we find that these objects are moderately luminous AGNs, making up ≈0.5% of the LBG population from $z \sim 3$ to ∼6.

Using our stacking procedure (see § 2), we detect X-ray emission from LBGs at $z \sim 3$ and an optically bright subset of LBGs at $z \sim 4$. X-ray count rates, derived from our soft-band detections and hard-band upper limits (3 σ), were used to constrain the spectral slopes of these LBGs. The 2.0–8.0 keV to 0.5–2.0 keV band ratio ($\Phi_{2.0-8.0\,\mathrm{keV}}/\Phi_{0.5-2.0\,\mathrm{keV}}$) is calculated to be less than 0.9 for *U* dropouts, corresponding to an effective photon index lower limit of $\Gamma > 0.8$. A consistent, less tightly constrained photon index is also derived for our bright B_{435} dropouts. This lower limit is consistent with our assumed $\Gamma = 2$ photon index, which is expected for galaxies with high star formation activity. The derived average 2.0–8.0 keV X-ray luminosities for these LBGs are ≈1.5 and 1.4×10^{41} ergs s^{-1} for *U* dropouts and bright B_{435} dropouts respectively, a factor of ≈5–10 times higher than for typical starburst galaxies in the local universe (e.g., M82; Griffiths et al. 2000). Furthermore, our LBGs are a factor of ≈2 less luminous in X-rays than those studied by B01 and N02.

Assuming that the X-ray luminosity functions of our individually undetected LBGs at high redshifts have functional forms similar to those of normal/starburst galaxies in the local universe, we can estimate the expected median X-ray luminosities for these LBGs. This is important because for a luminosity function with significant skewness, the median will differ from the mean. We have investigated this using the David et al. (1992, hereafter DJF92) sample of 71 normal/starburst galaxies in the local universe and find the mean to median X-ray luminosity ratio $L_X^{\mathrm{mean}}/L_X^{\mathrm{median}} \approx 5$. The mean 2.0–8.0 keV X-ray luminosity for these 71 galaxies is $\approx 6 \times 10^{40}$ ergs s^{-1}, a factor of ≈2.5 lower than the mean X-ray luminosities of our *U* dropouts and optically bright subset of B_{435} dropouts. If we assume that the $L_X^{\mathrm{mean}}/L_X^{\mathrm{median}}$ ratio for our LBGs is similar to that of the DJF92 sample, the corresponding median 2.0–8.0 keV X-ray luminosity would be $\approx 3 \times 10^{40}$ ergs s^{-1}.

The strong *U*-dropout signal allows investigation of the contribution of specific subsets to the photon statistics (see § 2.2 for details and Table 2 for results). We find that the optically luminous *U* dropouts contribute most of the X-ray flux ($\mathrm{S/N_{bright}} \approx 1.5\ \mathrm{S/N_{dim}}$). It is possible that the emission from rest-frame UV may be heavily obscured by dust, as would be expected if LBGs were a "scaled-up" population of ultraluminous infrared galaxies (Goldader et al. 2002). The X-ray–to–*B*-band mean luminosity ratios for these LBGs suggests that this is likely not the case, and the intrinsic dust attenuation from LBGs is similar to that expected for star-forming galaxies (see Seibert et al. 2002). We find that relatively asymmetric sources ($A > 0.1$) dominate the photon counts. However, the rest-frame *B*-band luminosities of these LBGs are somewhat elevated compared with sources of low asymmetry index (i.e., $A \leq 0.1$), and we therefore offer no further interpretation. No additional information was extracted from subsets of LBGs with differing concentration indices.

Recent investigations have found that hard X-ray emission associated with HMXBs can be used as a direct indicator of the SFR (e.g., Bauer et al. 2002; Ranalli et al. 2003; Grimm et al. 2003). If we assume that the majority of the X-ray emission from

our stacked detections of U and bright B_{435} dropouts is indeed from HMXBs, we expect the corresponding mean (median) star formation rates to be $\approx$10–30 $M_\odot$ yr^{-1} ($\approx$2–10 $M_\odot$ yr^{-1}).

The X-ray luminosities for star-forming galaxies (such as LBGs) are potential tracers of global star formation history (Lilly et al. 1996; Madau et al. 1996; Blain et al. 1999). A global estimate of the SFR can be implicitly drawn from these LBGs by considering the X-ray luminosity per unit B-band luminosity, L_X/L_B (mean quantities). This ratio should be interpreted with some caution because of the possible nonlinear relationship between L_X and L_B (i.e., $L_X \propto L_B^\alpha$). The power-law index (α) for this relation has been reported to range from $\approx$1 (DJF92; Fabbiano & Trinchieri 1985) to as high as $\approx$1.5 (Shapley et al. 2001) for galaxies in the local universe. We find that L_X/L_B shows suggestive evidence for evolution with redshift, as illustrated in Figure 5*a*. Here our U and bright B_{435} dropouts are plotted and compared with the results for normal galaxies at $z \approx 0$ (DJF92) and early-type spirals from $z \approx 0.05$ to 1.5 (Wu et al. 2005). From these data we infer a peak in L_X/L_B at $z \approx 1.5$–3.0, consistent with predictions of GW01. These results, while based on larger samples of galaxies, are consistent with the near-constancy of L_X/L_{UV} at $z \sim 1$ and $z \sim 3$ reported by N02 for Balmer break galaxies and LBGs, respectively. In this description the global SFR is expected to peak at $z \approx 2.5$–3.5. During this epoch, X-ray emission is observed as a result of contributions from HMXBs and supernovae. Shortly after the UV-luminous population evolves, X-ray emission will continue in the form of LMXBs, resulting in an increase in L_X/L_B.

When stacking LBGs at higher redshift, $z \sim 5$ and $\sim$6 (V_{606} and i_{775} dropouts, respectively), we do not obtain significant detections. The AGN contribution may be slightly more significant for these LBGs, where the *Chandra* exposures are only capable of detecting individual objects with 2.0–8.0 keV luminosities $\gtrsim 10^{43}$ ergs s^{-1} (implying that many Seyfert-type AGNs might not be individually detected at these redshifts). In light of these limits, we therefore place constraints on the average AGN content of these LBGs. The derived rest-frame 2.0–8.0 keV luminosity upper limits (3 σ) for the V_{606} and i_{775} dropouts are 2.8×10^{41} and 7.1×10^{41} ergs s^{-1}, respectively. Such upper limits are characteristic of bright starburst or low-luminosity Seyfert-type galaxies and are the tightest constraints yet to be placed on the X-ray properties of LBGs at $z \gtrsim 5$. For comparison, X-ray analyses of 44 LBGs at $z \sim 5$ (Bremer et al. 2004) and 54 LBGs at $z \sim 6$ (Moustakas & Immler 2004) constrain their average 2.0–8.0 keV X-ray luminosities to be less than 3×10^{42} and 7×10^{42} ergs s^{-1} (3 σ), respectively.

Figure 5*b* shows the overall L_X/L_B versus L_X results for both individually detected and stacked LBGs. Stacking analyses show that the individually undetected LBGs at $z \sim 3$, 4, 5, and 6 have L_X/L_B ratios characteristic of local starburst galaxies. Our individually detected LBGs have much larger L_X/L_B ratios, which are expected for X-ray–luminous AGNs.

We gratefully acknowledge support from Space Telescope Science Institute (STScI) grant HST-GO-09425.26-A and NSF CAREER award AST 99-83783 (B. D. L., W. N. B.), the Royal Society (D. M. A.), and NSF grant 03-07582 (D. P. S.). We thank Stefan Immler and Wentao Wu for useful discussions and development of software.

REFERENCES

Alexander, D. M., Aussel, H., Bauer, F. E., Brandt, W. N., Hornschemeier, A. E., Vignali, C., Garmire, G. P., & Schneider, D. P. 2002a, ApJ, 568, L85
Alexander, D. M. et al. 2003, AJ, 126, 539 (A03)
Alexander, D. M., Vignali, C., Bauer, F. E., Brandt, W. N., Hornschemeier, A. E., Garmire, G. P., & Schneider, D. P. 2002b, AJ, 123, 1149
Barger, A. J., Cowie, L. L., Capak, P., Alexander, D. M., Bauer, F. E., Brandt, W. N., Garmire, G. P., & Hornschemeier, A. E. 2003a, ApJ, 584, L61
Barger, A. J., et al. 2003b, AJ, 126, 632
Bauer, F. E., Alexander, D. M., Brandt, W. N., Hornschemeier, A. E., Vignali, C., Garmire, G. P., & Schneider, D. P. 2002, AJ, 124, 2351
Blain, A. W., Smail, I., Ivison, R. J., & Kneib, J.-P. 1999, MNRAS, 302, 632
Brandt, W. N., Hornschemeier, A. E., Schneider, D. P., Alexander, D. M., Bauer, F. E., Garmire, G. P., & Vignali, C. 2001, ApJ, 558, L5 (B01)
Bremer, M. N., Lehnert, M. D., Waddington, I., Hardcastle, M. J., Boyce, P. J., & Phillipps, S. 2004, MNRAS, 347, L7
Bruzual, G., & Charlot, S. 2003, MNRAS, 344, 1000
Capak, P., et al. 2004, AJ, 127, 180
Conselice, C. J. 2003, ApJS, 147, 1
Conselice, C. J., Bershady, M. A., & Jangren, A. 2000, ApJ, 529, 886
Conselice, C. J., Gallagher, J. S., III, & Wyse, R. F. G. 2002, AJ, 123, 2246
Cristiani, S., et al. 2004, ApJ, 600, L119
David, L. P., Jones, C., & Forman, W. 1992, ApJ, 388, 82 (DJF92)
Dickinson, M., et al. 2004, ApJ, 600, L99
Fabbiano, G., & Trinchieri, G. 1985, ApJ, 296, 430
Ghosh, P., & White, N. E. 2001, ApJ, 559, L97 (GW01)
Giacconi, R., et al. 2002, ApJS, 139, 369
Giavalisco, M. et al. 2004a, ApJ, 600, L103 (G04a)
———. 2004b, ApJ, 600, L93
Goldader, J. D., Meurer, G., Heckman, T. M., Seibert, M., Sanders, D. B., Calzetti, D., & Steidel, C. C. 2002, ApJ, 568, 651
Griffiths, R. E., Ptak, A., Feigelson, E. D., Garmire, G., Townsley, L., Brandt, W. N., Sambruna, R., & Bregman, J. N. 2000, Science, 290, 1325
Grimm, H.-J., Gilfanov, M., & Sunyaev, R. 2003, MNRAS, 339, 793
Ho, L. C., et al. 2001, ApJ, 549, L51
Hogg, D. W. 2000, preprint (astro-ph/9905116)
Hogg, D. W., Baldry, I. K., Blanton, M. R., & Eisenstein, D. J. 2002, preprint (astro-ph/0210394)
Hornschemeier, A. E., Brandt, W. N., Alexander, D. M., Bauer, F. E., Garmire, G. P., Schneider, D. P., Bautz, M. W., & Chartas, G. 2002, ApJ, 568, 82
Kim, D.-W., Fabbiano, G., & Trinchieri, G. 1992, ApJ, 393, 134
Lilly, S. J., Le Fèvre, O., Hammer, F., & Crampton, D. 1996, ApJ, 460, L1
Lockman, F. J. 2004, in Soft X-Ray Emission from Clusters of Galaxies and Related Phenomena, ed. R. Lieu & J. Mittaz (Dordrecht: Kluwer), in press (astro-ph/0311386)
Madau, P., Ferguson, H. C., Dickinson, M. E., Giavalisco, M., Steidel, C. C., & Fruchter, A. 1996, MNRAS, 283, 1388
Malhotra, S., Wang, J.-X., Rhoads, J. E., Heckman, T. M., & Norman, C. A. 2003, ApJ, 585, L25
Mobasher, B., et al. 2004, ApJ, 600, L167
Moustakas, L. A., & Immler, S. 2004, ApJL, submitted (astro-ph/0405270)
Nandra, K., Mushotzky, R. F., Arnaud, K., Steidel, C. C., Adelberger, K. L., Gardner, J. P., Teplitz, H. I., & Windhorst, R. A. 2002, ApJ, 576, 625 (N02)
Norman, C., et al. 2002, ApJ, 571, 218
Ptak, A., Serlemitsos, P., Yaqoob, T., & Mushotzky, R. 1999, ApJS, 120, 179
Ranalli, P., Comastri, A., & Setti, G. 2003, A&A, 399, 39
Reddy, N. A., & Steidel, C. C. 2004, ApJ, 603, L13
Schmidt, M., & Green, R. F. 1986, ApJ, 305, 68
Schneider, D. P., Gunn, J. E., & Hoessel, J. G. 1983, ApJ, 264, 337
Schreier, E. J., et al. 2001, ApJ, 560, 127
Seibert, M., Heckman, T. M., & Meurer, G. R. 2002, AJ, 124, 46
Shapley, A., Fabbiano, G., & Eskridge, P. B. 2001, ApJS, 137, 139
Shapley, A. E., Steidel, C. C., Pettini, M., & Adelberger, K. L. 2003, ApJ, 588, 65
Spergel, D. N., et al. 2003, ApJS, 148, 175
Stark, A. A., Gammie, C. F., Wilson, R. W., Bally, J., Linke, R. A., Heiles, C., & Hurwitz, M. 1992, ApJS, 79, 77
Steidel, C. C., Adelberger, K. L., Giavalisco, M., Dickinson, M., & Pettini, M. 1999, ApJ, 519, 1
Steidel, C. C., Giavalisco, M., Dickinson, M., & Adelberger, K. L. 1996, AJ, 112, 352
Szokoly, G. P., et al. 2004, ApJS, in press
Vignali, C., Bauer, F. E., Alexander, D. M., Brandt, W. N., Hornschemeier, A. E., Schneider, D. P., & Garmire, G. P. 2002, ApJ, 580, L105
Wang, J.-X., et al. 2004, ApJ, 608, L21
Wu, W., et al. 2005, in preparation
Zheng, W., et al. 2004, ApJS, 155, 73